SINGLE STREAM SHEAR LAYER AND THE VISCOUS SUPERLAYER

John F. Foss
Department of Mechanical Engineering
Michigan State University
East Lansing, Michigan, USA
foss@egr.msu.edu

Kyle M. Bade
Spray Analysis and Research Services
Spraying Systems Co.
Wheaton, Illinois, USA
kyle.bade@spray.com

Douglas R. Neal
LaVision Inc.
Ypsilanti, Michigan, USA
dneal@lavisioninc.com

Richard J. Prevost
LaVision Inc.
Ypsilanti, Michigan, USA
rprevost@lavisioninc.com

Scott C. Morris
Dept. of Aerospace and Mech. Eng.
University of Notre Dame
South Bend, Indiana, USA
smorris1@nd.edu

ABSTRACT

A single stream shear layer (SSSL) is bordered by two entraining boundaries: *i*) parallel entrainment on the high speed (U_0) side and *ii*) perpendicular entrainment on the low speed (V_e) side. The present study provides detailed PIV-based information on: *i*) the non-vortical/vortical boundary locations including the associated velocity magnitudes and the lengths of the convoluted borders and *ii*) the vortical properties and the stochastic width of the viscous super layer (VSL) for the low speed side as well as *iii*) the intermittency distribution. Access to the well resolved transverse vorticity values has avoided the problematic use of the "Non-Turbulent/Turbulent" designations to represent the border and the intermittency factor.

INTRODUCTION

A free turbulent shear flow (a domain of vortical fluid with a characteristic cascade of turbulent kinetic energy to the dissipative scales), that is bounded by an external free stream, will exhibit a propagating front where the external fluid is added to the sheared (vortical) fluid. Representative examples include: axisymmetric and planar jets and wakes. The present subject flow: a single stream shear layer, is distinctive since its boundaries involve parallel (high speed side at U_0) and perpendicular (low speed side at V_e) entrainment. As shown below, the present flow is further distinctive in that its low speed side entrainment fluid is operationally irrotational[1].

[1]A typical laboratory SSSL (see Hussain and Zaman, 1985; Liepmann and Laufer, 1947; Wygnanski and Fiedler, 1970; Dziomba and Fiedler, 1976; Foss, 1977) involves a prime mover that delivers the primary flow to the test section. Turbulence manipulators (Loehrke and Nagib, 1972)) in this flow path will deliver the high speed free stream fluid with a low free stream turbulence level. In contrast, the entrainment stream in these experiments was delivered to the test section with the residual turbulence level associated with the recycled shear layer fluid at the same pressure as that of the laboratory ambient. That is, manipulators cannot be added into the entrainment flow path without an auxiliary power source.

The vorticity transport equation (in the absence of non-barotropic effects):

$$\mathrm{D}\omega/\mathrm{D}t = \omega \cdot \nabla V + \nu \nabla^2 \omega \qquad (1)$$

shows that an initially non-vortical fluid dynamic particle can only gain vorticity by the direct action of viscosity. This fundamental observation led Corrsin (1943) followed by Corrsin and Kistler (1955) to identify the non-vortical to vortical transition as being associated with the physical phenomenon that he termed the "viscous super layer (VSL)". Since *high* Reynolds number implies small ν, he further reasoned that the length scale of the ∇^2 operator would be *small*. That is, that there would be a *sharp front* between the exterior and the interior fluid domains. The terminology adopted for this communication is to specify that sharp front as the border of the VSL; hereafter, ***border***. (Explicitly, the ***border*** exists between the non-vortical and the vortical fluid domains.) It is a two-dimensional feature of the flow which will be realized as a one-dimensional entity when revealed by a laser light sheet. The three-dimensional VSL is realized as a two-dimensional entity given its identification by the light sheet.

These considerations provide the essential context for the present paper. Five thousand particle image velocimetry (PIV) realizations of the low speed region of a large Reynolds number SSSL have been used to identify the ***border*** and the properties of the VSL in that subject flow. For emphasis, it is noted that the terminology: "Turbulent/Non-Turbulent Interface" is explicitly not used in the present communication albeit it is in common usage in technical publications. Such usage (see Attili et al., 2014; Watanabe et al., 2016; Da Silva and Taveira, 2010; Khashehchi et al., 2013; Westerweel et al., 2002) is considered to be problematic given the absence of a universally acknowledged definition of "turbulent". From an experimental standpoint, if the entrained fluid is not irrotational, then a more nuanced designation would be required to represent the ***border*** and the VSL. However, that new designation will not

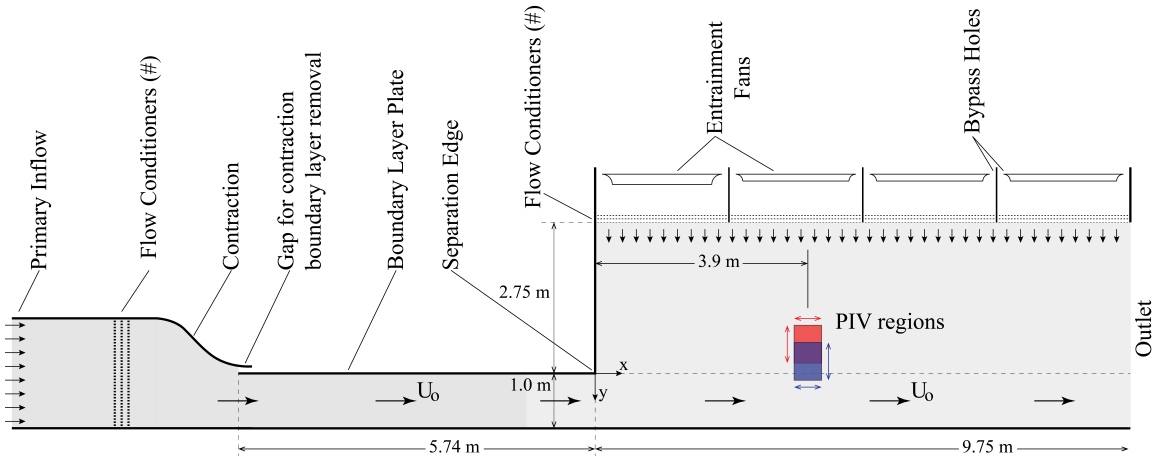

Figure 1: Plan view schematic of the single stream shear layer facility used for these experiments (uniform height of 2m). Noteworthy components as well as the PIV data regions are identified; (#) see Loehrke and Nagib, 1972.

be "turbulent/non-turbulent" without further criteria being given.

As a final introductory note, identifying the SSSL as an independent canonical free shear flow, independent from the two stream shear layer as U_2 approaches zero, was the subject of the investigation reported by Schmitt et al. (1986).

EXPERIMENTAL SETUP & METHODS

The Flow System

Figure 1 shows the experimental facility. The upstream fetch of the boundary layer plate was 5.74 m and the farther upstream (7.74m) turbulence manipulators for the primary flow were located where the flow path was 2.0 m wide. The uniform height of the facility was 2.0 m. The primary flow entered the test section with a width of 1.0 m and a velocity of 7.4 m/s. A 10 cm turbulent boundary layer ($R(\theta(0)) = 4.93 * 10^4$) was present at the separation lip. The entrainment flow was delivered into the test section using 4, 1.2 m diameter, fans followed by a honey comb and 3 screens, per the advice of Loehrke and Nagib (1972). The efficacy of this flow "smoothing" is evident in the vorticity observations. As documented in Morris and Foss (2003), the time-mean flow field was self-preserving by $x/\theta(0) = 200$. A rectangular domain, centered at $390\theta(0)$ and described in the next section, was used for the PIV observations. The PIV seed was introduced upwind from the entrainment fan that "fed" the imaged area.

The entrainment fans were controlled to deliver the entrainment velocity, V_e, at the self-preserving level: $V_e/U_0 = \mathrm{d}\theta(x)/\mathrm{d}x = 0.035$. Given the apparent origin for $\theta(x)$ from Morris and Foss (2003), the $\theta(x)$ values were known in the discussion of the vorticity observations presented below.

PIV Measurements

A two-camera imaging system was used to collect the PIV data. This system was comprised of two LaVision Imager sCMOS cameras (5.5 MP, 16-bit) and a 200 mJ Quantel Evergreen double-cavity Nd:YAG laser. The cameras were placed side-by-side to extend the effective field-of-view (FOV) for the measurements. This configuration resulted in two independent measurement planes that had an overlapped region between them. The flow was seeded using Di-Ethyl-Hexyl-Sebacat (DEHS) in a standard Laskin nozzle seeder that provided $1-2\mu$m particles. Data were acquired at 15 Hz and collected in 4 ensembles of 1250 image pairs resulting in 5000 independently measured PIV realizations for each of the two different camera configurations.

The data were processed using DaVis 8 (LaVision), which allows for multi-pass PIV correlations (deformed interrogation regions of decreasing size), as described in Smith and Neal (2016). The final pass used interrogation windows that were 32 × 32 pixels and 75% overlap, yielding a measurement cell size of $(1.56\ \mathrm{mm})^2$; hereafter "cell". The initial vector maps were post-processed using a universal outlier detection filter (Westerweel and Scarano, 2005). No additional smoothing or interpolation operations were implemented and any location where a vector was missing was left blank (i.e. no "filling" for missing vectors). The two individual vector maps were processed (and post-processed) individually and then stitched together by mapping the two vector maps onto a common grid and averaging the values in the overlapped region. The stitched vector maps resulted in a single FOV that was 700 mm × 500 mm with a vector grid of 320 × 449 vectors. The overlapped region was approx, 140 mm × 500 mm, or nominally 28% of the total measurement area.

Extraction of the ω_z Values

The regular grid of velocity values (each cell) makes it possible to obtain ω_z from the circulation (Γ) defined for the 3x3 array of cells that surround the subject location; this technique is made explicit in Bade and Foss (2010). The cyclic integral of $V \cdot \mathrm{d}s$ around the 8 incremental lengths surrounding the subject location is equated to the spatially averaged ω_z value over the area bounded by those 8 increments. That spatial average is then assigned to the center cell. The algorithm is repeated for all interior cells of the rectangular domain. The initial measurement represents ω_z for an area of 4 cells. Collapsing that to one cell can suppress maximum positive and negative ω_z values. However, that result is preferred with respect to the errors in a derivative based computation of ω_z that can be in error since it is unknown where in the cell the inferred velocity actually resides. As a result, each cell is represented by u,v,ω_z.

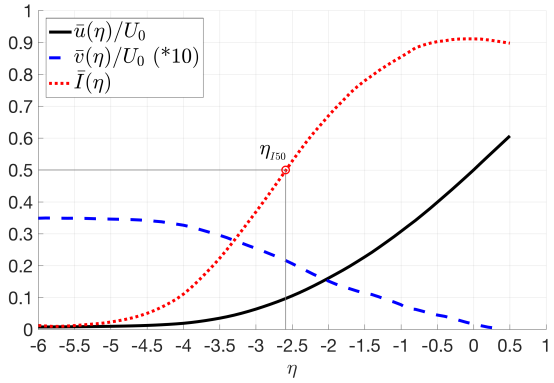

Figure 2: Mean streamwise & spanwise velocity and intermittency profiles; η_{I50}=-2.62, $u(\eta_{I50})/U_0$=0.0941 , and $v(\eta_{I50})/U_0$=0.0219.

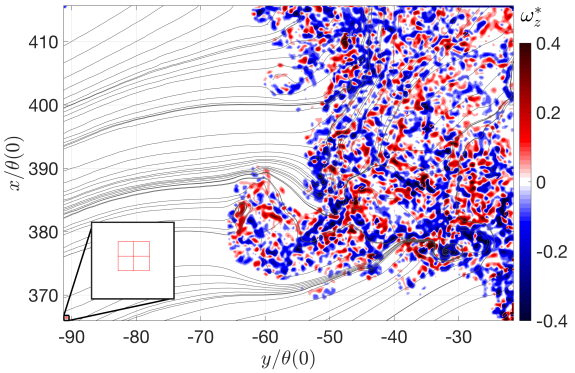

Figure 3: A representative vorticity field with an example 2x2 cell grid to demonstrate the spatial resolution of the PIV data.

VSL Border Identification Strategy

Equation 1 suggests the basis for the identification strategy. Namely, the algorithm will identify those locations in the ω_z field where the translating fluid dynamic particle can gain vorticity by viscous diffusion: $\nu\nabla^2\omega_z$. A non-zero, but a minimum value for that quantity is, of course, a necessary but not a sufficient condition for a ***border*** location. The present discussion will consider that quantity in its dimensional form since it represents the present experiment and not a universal quantity.

The strategy was implemented by first computing the $\nabla^2\omega_z$ magnitude (central difference method) at each interior location for each realization. Separate threshold levels (T.L.) of 1.0, 1.5, 2.0,... were then used to replace $\nabla^2\omega_z$ with an indicator function: IV, where IV = 0 indicates a value below the T.L. and IV = 1 indicates a value $\geq$T.L. The objective, at this stage of the strategy-implementation, was to determine candidate locations for the ***border***.

Every cell for each realization was assessed by its IV value and those of the surrounding 8 cells. A candidate cell was established if 4, 5, or 6 of the 9 cells (3x3 grid) had IV values of 1. A greater count suggested an "interior" cell whereas a lesser count suggested an "outer" cell. This initial sorting was followed by the definitive operation: establish the ***border*** for that realization as the longest contiguous path through the candidate locations that spanned the distance from $x_{\min}$ to $x_{\max}$. This step eliminated interior "lakes" and exterior "islands".

EXPERIMENTAL RESULTS & DISCUSSION

Basic Results

Figure 2 is for the reader's orientation. It presents the ensemble averaged (5,000 realizations) non-dimensional x and y component velocities and the intermittency function (I) as a function of η (where $\eta = (y - y_{1/2})/\theta(x)$). These data were obtained from the entire rectangular domain. (The $I(\eta)$ result is clarified below.)

Figure 3 provides one realization of the vorticity field. Using the experiment's length and velocity scales for the non-dimensionalization, $\omega_z^* = \omega_z\theta(0)/U_0$. The indicated values are representative of all 5000 realizations in that: *i*) an apparent ***border*** is present and *ii*) that relatively large values of ω_z are present. The small red square at the lower left corner of Figure 3 is a representative 2x2 array of interrogation cells. Their perimeter represents the integration path for Γ. Note that the u,v,ω_z values have been determined for each cell that is 1/4$^{\text{th}}$ the area of the 2x2 square. The ***border*** finding algorithm presented in the previous section was utilized for this and a number of other realizations with a common result as shown in Figures 4a-c. At a threshold level (T.L.) of 1 and 1.5, it is evident that the algorithm has *found* the residual vorticity from the manipulators; note especially that the T.L. 1.5 ***border*** trends toward the screens. This inference is substantiated with the data of Figure 5 that shows the ensemble average value of the vorticity-variance at the resolved ***border*** for each T.L value. The monotonic increase of the ordinate with increasing T.L. values supports the selection of T.L. = 2 for further processing of the PIV data. That is, the higher levels of the Figure 5 ordinate show that the ***border*** is too far into the vortical domain when T.L. > 2.

Characteristics of the *Border* and the VSL

The known ***border*** locations for the 5000 images allow a composite histogram of the ω_z values at the ***border*** to be defined; see Figure 6. Its small mean value is self-consistent with the understanding that vorticity propagates by diffusion from the interior to the ***border*** where it meets the convected irrotational fluid of the entrainment stream. The width of the distribution of the ω_z values (shown by the variance that is 12.2 times the mean value) indicates that both signs of ω_z are strongly present at the ***border***. On average, both the ***border*** and its vorticity filaments will be aligned in the z-direction for this planar flow field.

The known ***border*** locations also allow the in-plane velocity magnitude values to be known. Figure 7 presents the histogram of the ***border*** values: $q_b/V_e = (u^2 + v^2)^{1/2}/V_e$. Given that an inviscid streamline can be traced from each border point back to the third screen of the manipulator, it is evident that the *sink effect* of a low static pressure is responsible for the more than three-fold acceleration of the entrainment velocity. It is understood that the shearing effect at the ***border*** is responsible for the *fluid removal* that results in the low pressure. This behavior is clearly an important part of the entrainment process. The positively skewed distribution of values in Figure 7 show that some ***border*** locations experience quite low static pressure values.

Each ***border*** trajectory will cross the mid-x location (390 $\theta(0)$). In the event of more than one crossing, the following is carried out using only the central location. The η value of the crossing for that realization provides a reference condition for the relative length of the ***border***: L_η.

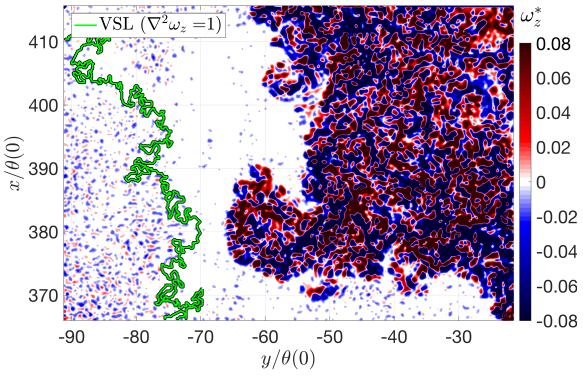

(a) T.L. = 1.0

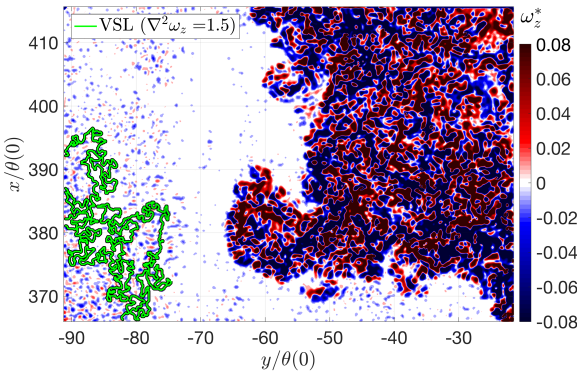

(b) T.L. = 1.5

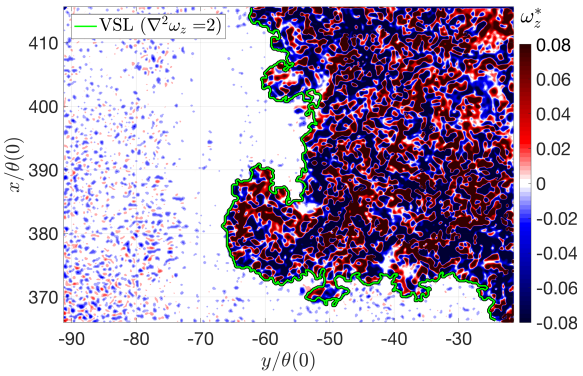

(c) T.L. = 2.0

Figure 4: A representative vorticity field with the ***border*** located using a T.L. of a) 1.0, b) 1.5, and c) 2.0.

That is, L_η is the length along the constant η trajectory from $x_{\min}$ to $x_{\max}$ within the data domain. The ***border*** length, L_b, for that realization is then made non-dimensional by L_η and the histogram of those values ($L_b^* = L_b/L_\eta$) is presented in Figure 8. Three moments of the associated population: mean, variance and skewness, are considered to be instructive in identifying the characteristics of the ***border***.

By definition, the ***border*** is a two-dimensional surface (one-dimensional in the plane of the PIV image) and the VSL (that is bordered) is a three-dimensional domain. The PIV image plane allows a two-dimensional representation of the VSL. The statistical width of the VSL was obtained by: *i*) locating 5 in-line ***border*** locations (either x or y) that defined a planar front to the ***border*** and then *marching inward* to form an ensemble of the vorticity values per *marching step*. The ensemble mean and variance of those values for the 5,000 realizations is shown in Figure 9. The "plateau" in the variance values is understood to provide a clear indication that the VSL exists between the ***border*** and the "plateau". It is further assumed that the "plateau" region represents the *fully turbulent region* where the measured ω_z is but one-component of the three-dimensional vorticity vector. The indicated nominally homogeneous condition then allows the dissipation of turbulence kinetic energy to be estimated:

$$\varepsilon = \nu(\omega \cdot \omega) \tag{2}$$

If the vortical motions were isotropic in the plateau region, then the Kolmogoroff microscale was $(\nu^3/\nu\ 3\langle\omega_z^2\rangle)^{0.25}$ or

$$\eta_\kappa = c_1(\nu/\tilde{\omega}_z)^{0.5} \tag{3}$$

where $c_1 = 3^{-0.25} \approx 0.76$. Conversely, if the vorticity vector has but one component (ω_z), then the Kolmogoroff microscale was larger; namely,

$$\eta_\kappa = (\nu/\tilde{\omega}_z)^{0.5} \tag{4}$$

These estimates of η_κ allow two more abscissa scales to be added to Figure 9.

The peak in the ω_z variance is understood to represent a transition between the dominance of that component and the three components of the plateau region. With that understanding, and with the consideration that the VSL exists between the ***border*** and the plateau, it is seen that the VSL is nominally 20 Kolmogoroff lengths wide.

SUMMARY

The present experiment is distinctive, if not unique, in terms of providing an irrotational entrainment stream at the border of the vortical shear layer. This feature allows the in-principle designation: vortical/non-vortical (cf the problematic "Turbulent/Non-Turbulent" designation) to identify the border of the VSL (viscous super layer) on the low speed side of a high Reynolds number single stream shear layer.

Five thousand PIV realizations of u,v,ω_z at each cell were obtained. The PIV field represented 449×320 cells per image, in y and x respectively, which was demonstrated to provide very good spatial resolution (see Figure 3).

Minimum values of $\nabla^2\omega_z$ (namely, 2 $[\mathrm{m^2s}]^{-1}$) were identified as candidate locations for the VSL ***border*** (see Figures 4 and 5). The ***border*** was then identified as the longest contiguous path from min-to-max streamwise locations of the PIV image. The two-dimensional ***border*** was revealed as a one-dimensional length in the PIV plane.

The ***border*** lengths were scaled on the diagonal length of the self-preserving mean velocity distribution (constant $\eta(x/\theta(0) = 390$ for each realization) in order to characterize the border convolutions. The mean, variance and skewness values of the normalized length, L_b^*, were: 2.98, 1.14 and 1.33 (see Figure 8).

The entrainment fluid accelerates from its "large" distance beyond the active shear layer to the ***border***. The normalized velocity magnitudes at the ***border***, q_b/V_e, for each

realization were collected into a histogram with the properties: mean, variance and skewness = 3.29, 2.04 and 1.39 (see Figure 7).

The three-dimensional VSL is revealed as two-dimensional region in the plane of the PIV images. It is identified by a distinctive rise in the variance of the vorticity from the ***border*** to a "plateau" region of nominally homogeneous turbulence. The latter allows an estimate of the Kolmogoroff length scale: η_K. The width of the VSL was determined to be nominally $20\eta_K$. The vorticity variance in the homogeneous region was nominally 2.5 times larger than that at the ***border*** with a non-dimensional magnitude of $\tilde{\omega_z}^* = \tilde{\omega_z}\theta(0)/U_0 = 0.068$.

The conventional intermittency factor (1 if vortical, 0 if non-vortical) was obtained and added to the ensemble mean velocity distributions. The target value for the self-preserving entrainment velocity (as driven by the entrainment fans) $V_e = 0.035U_0$, was obtained with very good precision. Figure 2 shows that the average border location is located at η=-2.62.

REFERENCES

Attili, A., Cristancho, J. and Bisetti, F. 2014 Statistics of the turbulent/non-turbulent interface in a spatially developing mixing layer. *Jour. of Turbulence* **15(9)**.

Bade, K.M. and Foss, J.F. 2010 Attributes of the large-scale coherent motions in a shear layer. *Exp. in Fluids* **49**, pp. 225-239.

Corrsin, S. 1943 Investigations of flow in an axially symmetric heated jet of air. NACA WR W-94, Washington, DC.

Corrsin, S. and Kistler, A.L. 1955 Free-stream boundaries of turbulent flows. NACA TR 1244, Washington, DC.

Da Silva, C. and Taveira, R. 2010 The Thickness of the turbulent/non-turbulent interface is equal to the radius of the large vorticity structures near the edge of the shear layer. *Physics of Fluids* **22**.

Dziomba, B. and Fiedler, H.E. 1976 Effect of Initial Conditions on Two-Dimensional Free Shear Layers. *Jour. of Fluid Mech.* **152**, pp. 419-442.

Foss, J.F. 1977 The effect of the laminar/turbulent boundary layer states on the development of a plane mixing layer. *Proc. 1st Inter. Symp. on Turb. Shear Flows*, Penn. State Univ., pp. 11-33.

Hussain, A.K.M.F. and Zaman, K.B.M.Q. 1985 An experimental study of organized motions in the turbulent plane mixing layer. *Jour. of Fluid Mech.* **159**, pp. 85-194.

Khashehchi, M., Ooi, A., Soria, J., and Marusic, I. 2013 Evolution of the turbulent/non-turbulent interface of an axisymmetric turbulent jet. *Exp. in Fluids* **54**, pp.1449.

Liepmann, H. and Laufer, J. 1947 Investigation of Free Turbulent Mixing. NACA TN 1257, Washington, DC.

Loehrke, R.I. and Nagib, H.M. 1972 Experiments on Management of Free Stream Turbulence. AGARD Report 598.

Morris, S.C. and Foss, J.F. 2003 Turbulent boundary layer to single-stream shear layer: the transition region. *Jour. Fluid Mech.* **494**, pp. 187-221.

Schmitt, T.P., Ali, S.K. and Foss, J.F. 1986 Relative Efficiencies of Parallel and Perpendicular Entrainment Flow Paths. *AIAA Journal* **24** 1443-4.

Smith, B.L. and Neal, D.R. 2016 Particle Image Velocimetry. Johnson, R.W. (Ed.). *Handbook of Fluid Dynamics* CRC Press, Chicago.

Watanabe, T., da Silva, C., Sakai, Y., Nagata, K., and Hayase, T. 2016 Lagrangian Properties of the entrainment across turbulent/non-turbulent interface layers. *Physics of Fluids* **28**.

Westerweel, J., Hofmann, T., Fukushima, C., and Hunt, J. 2002 The turbulent/non-turbulent interface at the outer boundary of a self-similar turbulent jet. *Exp. in Fluids* textbf33, pp. 873-878.

Westerweel, J. and Scarano, F. 2005 Universal outlier detection for PIV data. *Exp. in Fluids* **39(6)**, 1096-1100.

Wygnanski, I. and Fiedler, H.E. 1970 The Two-Dimensional Mixing Region. *Jour. of Fluid Mech.* **41(2)**, pp. 327-361.

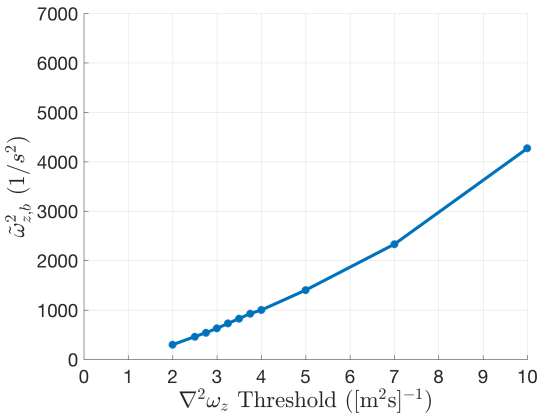

Figure 5: Threshold Level (T.L.) evaluation

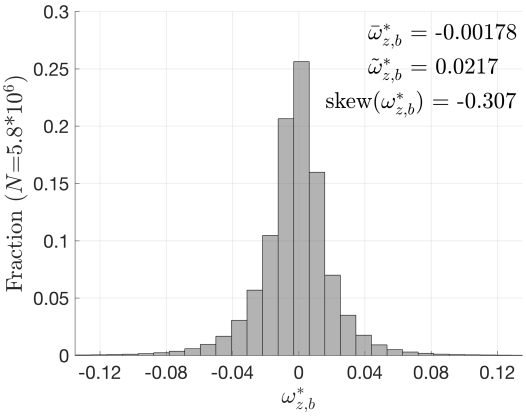

Figure 6: Histogram of non-dimensional vorticity at the ***border*** and related statistics

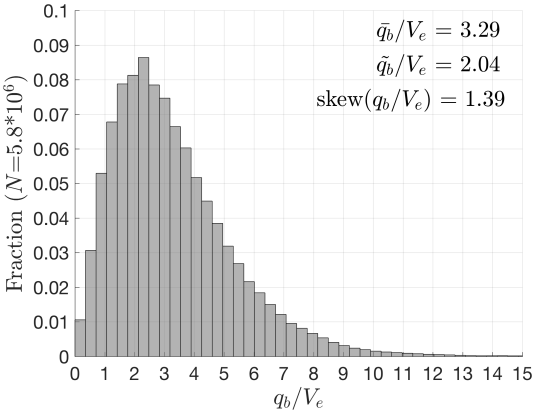

Figure 7: Histogram of non-dimensional velocity magnitude at the ***border*** and related statistics

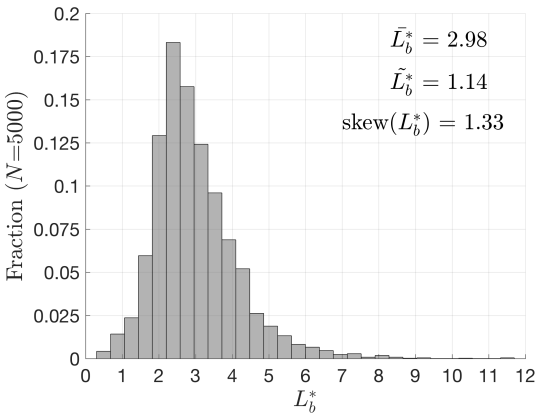

Figure 8: Histogram of normalized ***border*** lengths and related statistics

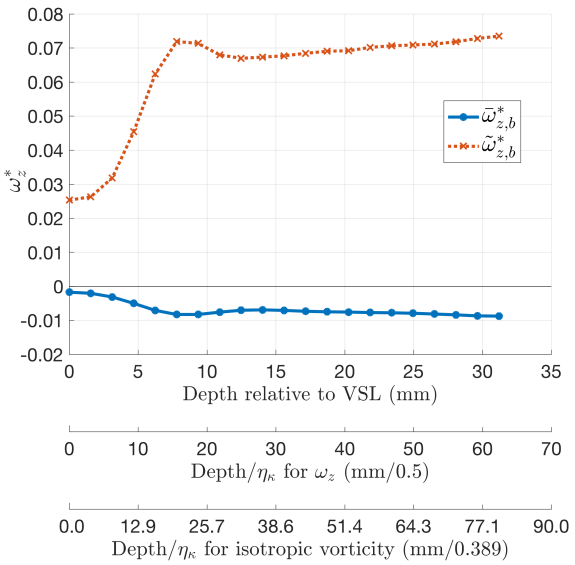

Figure 9: Vorticity (mean and variance) distributions referenced to the ***border***